

PAPER • OPEN ACCESS

Experimental exploration of the amphoteric defect model by cryogenic ion irradiation of a range of wide band gap oxide materials

To cite this article: J Borgersen *et al* 2020 *J. Phys.: Condens. Matter* **32** 505701

View the [article online](#) for updates and enhancements.



IOP | ebooks™

Bringing together innovative digital publishing with leading authors from the global scientific community.

Start exploring the collection—download the first chapter of every title for free.

Experimental exploration of the amphoteric defect model by cryogenic ion irradiation of a range of wide band gap oxide materials

J Borgersen^{1,2,6} , L Vines^{1,2} , Y K Frodason^{1,2} , A Kuznetsov^{1,2} ,
H von Wenckstern³ , M Grundmann³ , M Allen⁴ , J Zúñiga-Pérez⁵  and
K M Johansen^{1,2} 

¹ Department of Physics, University of Oslo, Norway

² Centre for Materials Science and Nanotechnology, University of Oslo, Norway

³ Felix Bloch institute for Solid State Physics, Fakultät für Physik und Geowissenschaften, Universität Leipzig, Germany

⁴ Department of Electrical and Computer Engineering, University of Canterbury, New Zealand

⁵ Centre de Recherche sur l'Hétéro-Epitaxie et ses Applications (CRHEA), CNRS, Université Côte d'Azur, France

E-mail: jonborg@fys.uio.no

Received 5 May 2020, revised 9 July 2020

Accepted for publication 5 August 2020

Published 23 September 2020




CrossMark

Abstract

The evolution of electrical resistance as function of defect concentration is examined for the unipolar *n*-conducting oxides CdO, β -Ga₂O₃, In₂O₃, SnO₂ and ZnO in order to explore the predictions of the amphoteric defect model. Intrinsic defects are introduced by ion irradiation at cryogenic temperatures, and the resistance is measured in-situ by current–voltage sweeps as a function of irradiation dose. Temperature dependent Hall effect measurements are performed to determine the carrier concentration and mobility of the samples before and after irradiation. After the ultimate irradiation step, the Ga₂O₃ and SnO₂ samples have both turned highly resistive. In contrast, the In₂O₃ and ZnO samples are ultimately found to be less resistive than prior to irradiation, however, they both show an increased resistance at intermediate doses. Based on thermodynamic defect charge state transitions computed by hybrid density functional theory, a model expanding on the current amphoteric defect model is proposed.

Keywords: Ga₂O₃, In₂O₃, defect, irradiation, amphoteric defect model

 Supplementary material for this article is available [online](#)

(Some figures may appear in colour only in the online journal)


1. Introduction

The wide band gap semiconducting oxide materials exhibit a plethora of interesting properties, including optical transparency, high electrical conductivity and breakdown field

strength, piezoelectricity etc., making them highly desirable in a range of devices [1–5]. Several electrical properties of these materials, e.g. the maximum achievable carrier concentration, surface accumulation/depletion of electrons and propensity for either *p*- or *n*-type doping are related to their intrinsic and extrinsic defects [6]. Fundamental knowledge of the defects and their behaviour is thus of scientific interest, and also paramount for device fabrication.

A model frequently used for describing the formation of intrinsic defects in semiconductors is the amphoteric defect

⁶ Author to whom any correspondence should be addressed.

 Original content from this work may be used under the terms of the [Creative Commons Attribution 4.0 licence](#). Any further distribution of this work must maintain attribution to the author(s) and the title of the work, journal citation and DOI.

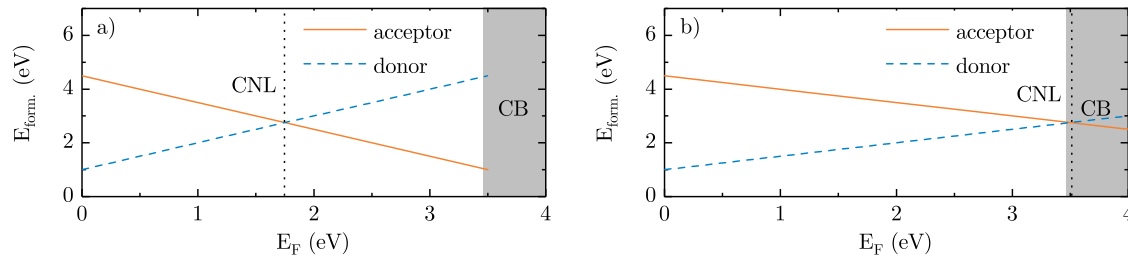


Figure 1. Generic formation energies for an intrinsic donor and acceptor as function of Fermi level relative to the valence band. The shaded bar on the right illustrates the conduction band. The charge neutrality level (CNL) lies at the intersection between the donor and the acceptor formation energies and is shown as a dotted line. Two cases are illustrated, (a) a conventional semiconductor with the CNL close to midgap, and (b) a material with the CNL within the conduction band.

model (ADM) [7]. One of the main assumptions of the model is that a native defect generally can exist in several charge states, and may act either as a donor or as an acceptor (amphoteric behaviour). Furthermore, the charge state of a defect is governed by the Fermi level (E_F) and its probability of formation is determined by the formation energy. For donor states, the formation energy increases with E_F while the converse is true for acceptors. As the electrical effect of a donor (acceptor) is to increase (decrease) the Fermi level, introduction of intrinsic defects tends to shift E_F towards a level referred to as the charge neutrality level (CNL). In other words, if $E_F < \text{CNL}$ donor like states will preferentially form, whereas if $E_F > \text{CNL}$ acceptor like states will be favoured. On an energy scale, the CNL is located at the point where the formation energy of the most stable intrinsic donor equals that of the most stable intrinsic acceptor, as shown for a typical wide band gap material in figure 1(a). For illustrative purposes, the figure shows a single donor and acceptor pair having the lowest formation energies throughout the band gap. In practice this need not be the case and several defects may dominate in various regions of the gap. If a sufficiently high defect concentration is introduced, the Fermi level is pinned at the CNL and further generation of defects will not yield any net change in the carrier concentration.

The CNL of a material can be estimated by several theoretical approaches, and quantitatively the predicted position will depend on the details of the computation. One approach is to calculate the formation energies of all relevant intrinsic defects and, in line with the above reasoning, estimate the CNL as lying at the intersection of the formation energies of the dominant donor and acceptor states [8]. The defect states tend to be highly localized in real space and thus have an extended character in k -space. Consequently, a different route to obtaining the CNL is to calculate the energies of the valence and conduction band edges at all points of the Brillouin zone (BZ). From the band edges the local band gap at all points of the BZ can be determined, and by averaging the midgap value across the BZ an estimate of the CNL is obtained [9–11]. In practical calculations a choice of the relevant k -points at which to evaluate the band edges must be made. Several schemes are discussed in [12] and references therein. As a side note, it has been found that the donor/acceptor transition level of hydrogen can also be used as an estimate of the CNL in many materials [13].

For materials where both the valence and conduction band have low dispersion throughout the Brillouin zone the averaged midgap energy discussed above is close to the middle of the fundamental band gap, E_g , defined as the energy difference between the conduction band minimum (CBM) and valence band maximum (VBM). Most conventional semiconductors, including Si, Ge, and most binary III-Vs fit this description, and consequently their CNLs are found to lie well within the band gap as illustrated in figure 1(a) [7, 11, 13–15].

Interestingly, density functional theory (DFT) computations have predicted that certain more ionic materials, e.g. CdO, InN, In_2O_3 , SnO_2 and ZnO should, due to significant dispersion of their conduction bands, have CNLs above their respective conduction band minima, as illustrated in figure 1(b). This would allow the existence of high carrier concentrations before the introduced defects begin to self compensate the material, thereby partly explaining their surprisingly high conductivities [12, 16, 17]. For CdO and In_2O_3 these predictions have found experimental support by x-ray photoelectron spectroscopy, infrared reflectivity and Hall effect measurements of doped or room temperature ion irradiated samples, indicating that the intrinsic defects are donors even when the samples are heavily n -type [9, 10, 18].

A recent report [19] on the electrical properties of low temperature ion irradiated In_2O_3 , however, shows indications of a more complex defect evolution than what was found earlier [10]. Also, a range of elements implanted in ZnO at room temperature or above have all been found to considerably increase the resistivity of the samples, in contrast to the predicted behaviour for a material with the charge neutrality level positioned within the conduction band [20, 21].

These discrepancies merit further studies of the defect evolution in semiconducting oxide materials and in this work we investigate and compare the influence of defect concentration on the electrical properties of CdO, $\beta\text{-Ga}_2\text{O}_3$, In_2O_3 , SnO_2 and ZnO thin films. Controlled defect concentrations are introduced by low temperature ion irradiation, i.e. ion implantation at energies sufficient for allowing the incident ions to travel through the film of interest and into the substrate. This leaves a cascade of controllable concentration of intrinsic defects in the thin-film material of interest. At select doses, the resistivity of the sample is probed by *in situ* current–voltage (IV) measurements. Correlating these measurements with defect

Table 1. Deposition technique, nominal film thickness, substrate material, dimensions, dopant as well as room temperature carrier concentration before ($n_{\text{as dep.}}$) and after ($n_{\text{irr.}}$) irradiation for all the examined samples. For the deposition techniques, MBE refers to molecular beam epitaxy, while PLD refers to pulsed laser deposition.

Material	Deposition	Thickness (nm)	Substrate	Size (mm)	Dopant	$n_{\text{as dep.}}$ (cm^{-3})	$n_{\text{irr.}}$ (cm^{-3})
CdO	MBE	150	r-Al ₂ O ₃	5 × 5	none	1.5×10^{19}	1.6×10^{20}
Ga ₂ O ₃	PLD	600	c-Al ₂ O ₃	10 × 10	1% Si	9.5×10^{18}	—
In ₂ O ₃	PLD	800	c-Al ₂ O ₃	10 × 10	none	1.1×10^{19}	6.0×10^{19}
SnO ₂	MBE	150	r-Al ₂ O ₃	5 × 5	Sb	2.0×10^{18}	—
ZnO	MBE	180	c-Al ₂ O ₃	5 × 5	none	1.6×10^{17}	4.6×10^{18}

charge states and transition levels calculated by hybrid density functional theory we propose a defect generation model which expands on the previously introduced amphoteric defect model.

2. Experiments

Semiconducting CdO, Ga₂O₃, In₂O₃, SnO₂ and ZnO films of thickness in the range of 150–800 nm were grown on c- or r-plane sapphire substrates by pulsed laser deposition (PLD) or molecular beam epitaxy (MBE), as summarized in table 1. The CdO, In₂O₃ and ZnO films were nominally undoped, while the Ga₂O₃ and SnO₂ samples were doped with Si or Sb, respectively. 100 nm thick aluminium contacts were deposited on top of 10 nm titanium adhesion layers in each corner of the samples. The depositions were made by electron beam evaporation in an Angstrom Engineering EvoVac loaded with metal pellets of at least 99.99% purity. The base pressure before starting the evaporation was 2×10^{-6} torr, and the Ti and Al were deposited sequentially without breaking vacuum.

Prior to irradiation, temperature dependent Hall effect measurements were conducted in the van der Pauw geometry using a Lakeshore 7604 Hall measurement system. The applied magnetic field was 10 kG, and all samples were measured over a temperature range from 20 to 300 K in steps of 10 K. The Hall scattering factor was assumed to be unity for all measurements.

For the ion irradiation, Si²⁺ ions were accelerated to an energy of 3 MeV in an NEC Tandem ion implanter. The implantation chamber was evacuated to $<5 \times 10^{-7}$ torr and, in order to limit defect diffusion and dynamic annealing, the samples were cooled to 50 K (Ga₂O₃ and In₂O₃) or 70 K (CdO, SnO₂ and ZnO) using a closed cycle helium cryostat. From Monte Carlo simulations using the SRIM code [22], the ions are predicted to have a projected range of approximately 1.5 μm , i.e. well within the substrate for all samples, and this was verified using secondary ion mass spectrometry. Any observed changes in the films should thus be caused only by the intrinsic defects induced by the ion beam, and not by the silicon ions. *IV* measurements were performed across the surface diagonal of the samples at a range of irradiation doses up to $3 \times 10^{16} \text{ cm}^{-2}$ (CdO, SnO₂, ZnO) or 10^{17} cm^{-2} (Ga₂O₃, In₂O₃) with a Keithley 6487 voltage source/picoammeter using bias voltages in the range (+/−) 2 V.

Following the final irradiation, the samples were heated to room temperature before a temperature dependent Hall effect measurement was performed using the same parameters as described above.

To evaluate the electrical behaviour of native defects in ZnO, defect calculations were performed using the Heyd–Scuseria–Ernzerhof (HSE) [23] screened hybrid functional and the projector augmented wave method [24], as implemented in the VASP code [25]. The fraction of screened Hartree–Fock exchange, α , was set to 37.5%, which results in an accurate description of the experimental band gap and lattice parameters of ZnO [26]. Thermodynamic charge-state transition levels of defects were calculated by following the standard formalism described in [27].

For charged defects we applied the anisotropic [28] Freysoldt–Neugebauer–Van de Walle correction [27]. Defect calculations were performed using a 96-atom supercell, a plane-wave basis set with an energy cutoff of 500 eV, and a special k -point at $(\frac{1}{4}, \frac{1}{4}, \frac{1}{4})$. For defects involving V_O, however, a larger 192-atom supercell was required to ensure converged energy levels, as discussed in more detail elsewhere [29, 30]. Ionic relaxations were performed until the forces were reduced to less than 20 meV Å^{−1}, and spin-polarization was included.

3. Results and discussion

The results from the temperature dependent Hall effect measurements conducted before and after irradiation are presented in figure 2. Before irradiation all the studied samples have carrier concentrations (n) varying only very weakly with temperature with no sign of carrier freeze out. The strong positive temperature (T) dependence of the mobilities (μ) of SnO₂ and in particular ZnO indicate that these films are non-degenerate and that their carrier transport is limited by ionized impurity scattering [31]. The mobility of the In₂O₃ sample is seen to follow $\mu(T) \propto T$, indicating that the sample is degenerate with transport limited by grain boundary scattering [32]. For the lowest temperatures, the carrier concentration of both SnO₂ and ZnO seems to increase slightly. This is attributed to some form of parallel conduction either at the surface, or at the TCO/substrate interface [33, 34]. For CdO the negative temperature dependence of the mobility indicates that phonons are the dominant scattering mechanism, but also here a parallel conduction pathway could be present [35]. For Ga₂O₃ the mobility is seen to increase slowly with temperature, but at a lower rate than the $\mu \propto T^{3/2}$, which is expected for purely ionized impurity scattering in a non-degenerate material. A possible explanation for this temperature dependence could be that both ionized impurities and phonons together limit the carrier transport, possibly also aided by grain boundary scattering.

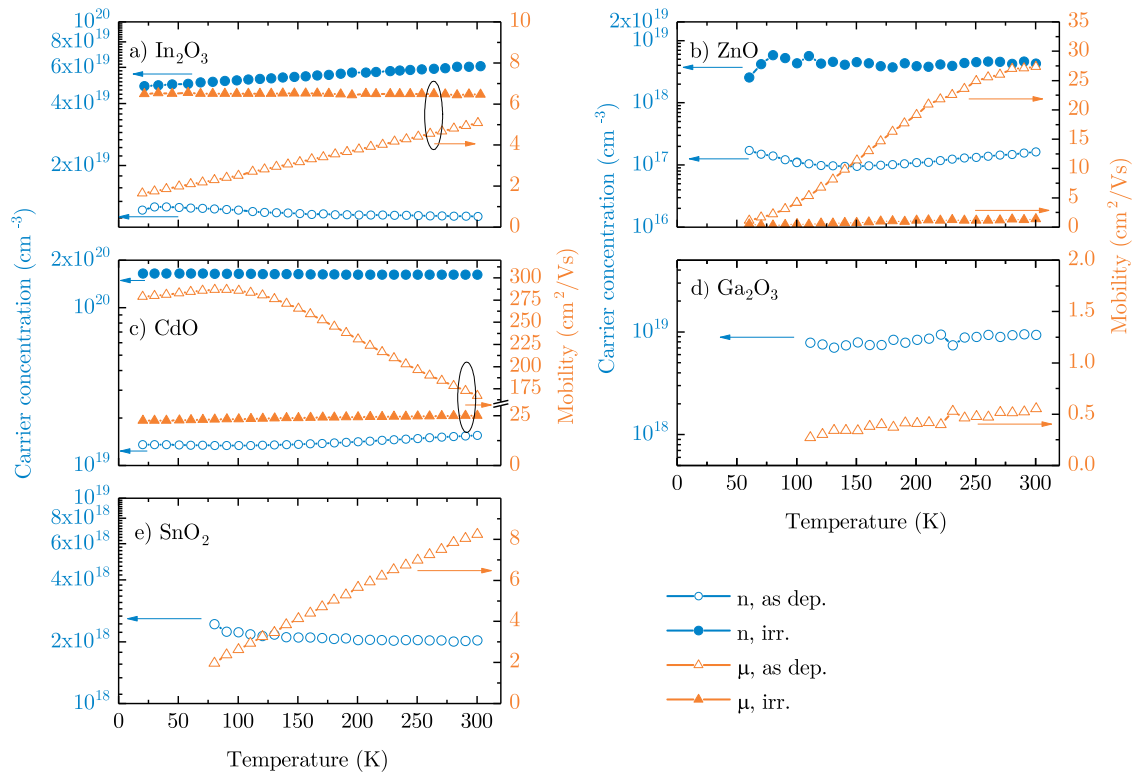


Figure 2. Temperature dependent Hall effect measurements before (open symbols) and after (filled symbols) irradiation of CdO, In₂O₃ and ZnO, as well as before irradiation of Ga₂O₃ and SnO₂. The carrier concentrations (n , blue) and mobilities (μ , orange) are plotted against the left and right vertical axis, respectively, and the legend applies to all the panels.

After irradiation to the maximum dose available in our setup, the carrier concentrations of CdO, In₂O₃ and ZnO have all increased compared to their as-deposited values. The strongest relative change is found in ZnO which increases from $n = 1.6 \times 10^{17} \text{ cm}^{-3}$ to $4.3 \times 10^{18} \text{ cm}^{-3}$ at room temperature, while the carrier concentrations of CdO and In₂O₃ increase from 1.6×10^{19} and $1.1 \times 10^{19} \text{ cm}^{-3}$ to 1.6×10^{20} and $6 \times 10^{19} \text{ cm}^{-3}$, respectively. Due to their high resistivities, Hall effect measurements on the Ga₂O₃ and SnO₂ samples were, unfortunately, not possible after irradiation.

For CdO and ZnO, the irradiation causes a considerably reduced mobility with a weak positive temperature dependence, suggesting that grain boundary scattering and/or other structural defects are the dominant scattering mechanisms. This is consistent with earlier work on the mobility of CdO [36]. The mobility of In₂O₃ on the other hand is, interestingly, found to increase after the irradiation. The increased carrier concentration and a temperature independent mobility, maintaining a value of $6.5 \text{ cm}^2 (\text{V s})^{-1}$ throughout the measured temperature range, indicates that the irradiation has rendered the material degenerate. Furthermore, the increase in mobility could imply a decreased concentration of compensating defects.

To relate the carrier concentrations found from the Hall effect measurements to the defect charge state transition levels and predicted CNLs we calculate the Fermi level of each material in its as-deposited state by iteratively solving the Fermi–Dirac integral numerically [37]. The effective masses

Table 2. Band gaps (E_g), effective masses (m^*), and Fermi levels (E_F) relative to the VBM. The Fermi levels were calculated from the room temperature Hall effect carrier concentrations by iterative numerical integrations of the Fermi–Dirac integral [37]. The band gaps are taken from [1, 5, 32, 38, 39] and the effective masses from [1, 32, 39–41].

	CdO	Ga ₂ O ₃	In ₂ O ₃	SnO ₂	ZnO
E_g (eV)	2.31	4.80	2.79	3.35	3.37
m^* (m_c)	0.26	0.28	0.18	0.30	0.30
E_F (eV)	2.39	4.85	2.88	3.34	3.29

used in the calculations along with the band gaps of the materials and their calculated Fermi levels are presented in table 2. This shows that the CdO, Ga₂O₃ and In₂O₃ samples are degenerate, while the SnO₂ and ZnO are not. Due to the relatively low carrier concentrations in the as deposited samples, the conduction bands of the samples are assumed parabolic [42].

Figure 3 shows the resistances calculated from the IV -measurements as functions of displacement damage dose (D_d) for all the investigated samples. The top horizontal axis shows an approximate vacancy concentration for ZnO. This was calculated from the accumulated ion dose and vacancy profiles simulated using SRIM [22], where the displacement energies of zinc and oxygen were set to 34 and 44 eV, respectively [43]. The strong dynamic annealing of ZnO [21] was accounted for by assuming that only 1% of the generated vacancies survived immediate recombination [44]. The displacement damage dose shown on the bottom x -axis is the product of the

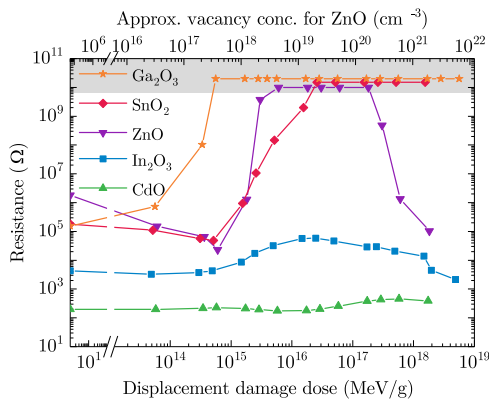


Figure 3. Resistance as function of accumulated displacement damage dose (D_d) measured at low temperature *in situ* between each irradiation step with the ion beam blanked. The datapoints plotted in the grey shaded region are outside the measurement range of our instrument.

ion dose and the non-ionizing energy loss (NIEL), which was calculated from SRIM simulations according to the procedure described in [45]. For these calculations, the displacement energies of zinc and oxygen in ZnO were set to 34 and 44 eV, as before. As reliable values are not readily available for all the studied materials, the displacement energies for both cations and oxygen in all the other samples were set to 15 eV, a common value for semiconductors [19, 46, 47]. The SRIM simulations were run for 20 000 primary ions and to avoid surface effects the 10 data points closest to the surface were discarded. The resulting NIEL values were 57.2, 56.2, 49.1, 51.7 and 60.6 MeV cm² g⁻¹ for CdO, Ga₂O₃, In₂O₃, SnO₂ and ZnO, respectively. Recalculating the NIEL for ZnO with 15 eV displacement energies for both Zn and O gives a value of 65.6 MeV cm² g⁻¹.

As the dimensions of the samples do not change between measurements, and assuming that the resistance of the contacts remains constant, any observed change in resistance is necessarily caused by a change in resistivity, i.e. a change in carrier concentration and/or mobility of the samples. The resistivity of In₂O₃ follows the same trend as observed in a recent paper by Vines *et al* [19]. At displacement damage doses below $\sim 5 \times 10^{13}$ MeV g⁻¹, the resistivity shows a minor decrease, followed by a stronger increase between $\sim 5 \times 10^{13}$ and 2.5×10^{16} MeV g⁻¹. At even higher displacement damage doses the resistivity again starts to decrease, and does not seem to stabilize at any ultimate value within the studied dose range. At the last datapoint, corresponding to a displacement damage dose of 4.9×10^{18} MeV g⁻¹, the sample has a lower resistivity than in its as-deposited state.

For Ga₂O₃ the resistivity increases monotonically, and for displacement damage doses greater than 3.4×10^{14} MeV g⁻¹ the resistance is beyond the measurement range of our setup, indicated by the shaded region along the top of figure 3. The immeasurably high resistance is retained until at least a displacement damage dose of 5.6×10^{18} MeV g⁻¹, confirming and extending the findings in [19], where the same behaviour was observed but the irradiation was aborted after an ion dose of 10^{14} cm⁻², corresponding to $D_d \sim 5.6 \times 10^{15}$ MeV g⁻¹.

In a recent report, proton irradiation of Ga₂O₃ to doses $\geq 2 \times 10^{13}$ cm⁻² has also been shown to decrease the carrier concentration dramatically, to the point that no response is obtained in capacitance-voltage measurements [48]. Subsequent heat treatment at temperatures of ~ 180 – 380 °C were found to greatly recover the carrier concentration, and the required temperature for recovery correlated positively with the irradiation dose. For our Ga₂O₃ sample irradiated to a displacement damage dose of 5.6×10^{18} MeV g⁻¹, no sign of electrical recovery was observed after annealing at temperatures up to 900 °C in air. We attribute this to the higher defect concentration introduced in our experiment.

The SnO₂ and ZnO samples qualitatively exhibit an intermediate behaviour compared to Ga₂O₃ and In₂O₃. Both display an initial, slow decrease in resistivity for displacement damage doses below 5×10^{14} MeV g⁻¹, followed by a rapid increase for doses up to at least 1.8×10^{16} MeV g⁻¹ (ZnO) or 2.6×10^{16} MeV g⁻¹ (SnO₂). Like Ga₂O₃, the SnO₂ sample remains highly resistive throughout the remainder of the dose range, whereas the ZnO sample behaves more like In₂O₃, showing a monotonically decreasing resistivity after a displacement damage dose of 1.8×10^{17} MeV g⁻¹. Kucheyev *et al* have previously observed a similar behavior for ZnO [20, 49]. They attributed the decreasing resistivity at high doses to the onset of hopping conduction [50], but this was not discussed in further detail in their work. Using Arrhenius plots of the measured resistivities before and after irradiation (not shown) we examined whether conduction by pure- or phonon-assisted hopping is likely to take place in our samples. No evidence of such conduction mechanisms was found for any sample, however the temperature dependences of the resistivities were too weak for the analysis to be conclusive.

The CdO sample exhibits a remarkably dose independent resistivity throughout the range. A minor drop in resistivity can be observed after a displacement damage dose of about 5.8×10^{15} MeV g⁻¹ followed by a slight increase to a peak at 5.8×10^{17} MeV g⁻¹ and at the last data point the resistivity again seems to decrease. Room temperature ion irradiation experiments on CdO have previously shown monotonic increases in the carrier concentration with increasing dose until saturating at 2.2×10^{20} cm⁻³ or 5×10^{20} cm⁻³ [9, 18]. This was interpreted as a consequence of the charge neutrality level being located above the conduction band minimum in CdO, and that the irradiation induced defects pushes the Fermi level towards the CNL. For CdO specifically, such an explanation could well fit our results presented in figures 2 and 3. The results for In₂O₃, SnO₂, and ZnO on the other hand, do not seem to fit the model. In particular, the facts that the resistivities neither change monotonically, nor stabilize at any ultimate value does not seem to fit with the idea of the CNL position being a reliable predictor of the outcome of a low temperature ion irradiation experiment in general. An underlying assumption of the charge neutrality model is that the stability and probability of formation of a given defect species is determined by its formation energy. Although the introduction of a specific species is easily accommodated in theoretical computations, and despite its appealing simplicity, we

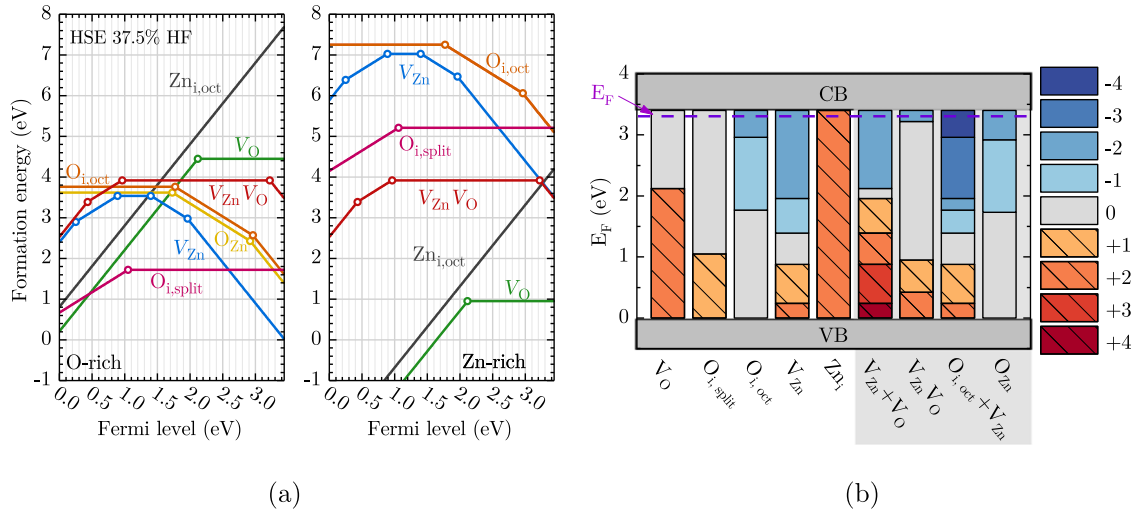


Figure 4. Thermodynamic defect charge state transition levels in ZnO. In (a) plotted in the conventional fashion as function of formation energy. The calculations for the zinc and oxygen vacancies were first published in [52], while the data for the $V_{Zn}V_O$ divacancy are published in [30]. Panel (b) shows the same dataset, but plotted in a more suitable way for the following discussion. Here, VB and CB refers to the valence- and conduction band minima, respectively, and the purple dashed line below the CB represents the calculated Fermi level of the as-deposited sample, as given in table 2. The columns labelled $V_{Zn} + V_O$ and $O_{i,oct} + V_{Zn}$ show the sum of the charge states of the individual point defects, while the columns $V_{Zn}V_O$ and O_{Zn} show the states for the complexes as calculated by DFT. The data for V_{Zn} and V_O , and $V_{Zn}V_O$ are reused from [30, 52], respectively, with permission.

question whether such a model is generally capable of describing the outcome of an ion irradiation experiment.

In order to understand the detailed process of defect introduction, a short review of the ion irradiation process is relevant. When a primary ion hits an atom in the sample, the atom may be ejected from its lattice site into an interstitial position, thus creating a Frenkel pair. During irradiation, this Frenkel pair generation takes place on each of the sublattices of the sample in a random process [51]. The defect generation mainly depends on the energy of the ion beam, mass of the ion species and the displacement energies of the different sublattices of the sample. Due to the high energy of the incident ion, the formation energies of the individual defects are expected to play only a negligible role in their formation probability, but may still be relevant for their thermal stability. Although they may, in principle, be formed in any allowed charge state, each defect will quickly accept or donate electrons until it is in the most favourable charge state, as governed by the Fermi level.

To explain the observed dose dependence of the resistivity shown in figure 3, we assume that the primary 3 MeV Si^{2+} ions are sufficiently energetic to produce Frenkel pairs at both the cation and anion sublattices. As our experiments are performed at low temperatures, clustering of the primary defects due to diffusion and defect reactions are expected to be suppressed for low irradiation doses. In the following the details of the defect generation will be discussed for each material separately, starting with ZnO.

3.1. ZnO

Thermodynamic charge states and transition levels for the intrinsic point defects in ZnO, as calculated by hybrid functional DFT, are illustrated in figure 4. Panel (a) is a conventional formation energy diagram showing the favoured charge

state and formation energy of the defects. In panel (b) the formation energy is discarded to highlight the information needed for the following discussion, namely the charge states as functions of Fermi level position. In addition to the point defects, two small complexes, the divacancy ($V_{Zn}V_O$) [30] and the oxygen antisite (O_{Zn}), are shown. The shaded regions represent the valence- (VB) and conduction bands (CB), and the estimated Fermi level before irradiation is indicated by the dashed line. Based on these predictions, introducing a Frenkel pair on the zinc sublattice in *n*-type ZnO will not yield any net change in the carrier concentration as the zinc vacancy is doubly negative for Fermi level positions >2 eV above the valence band, while the interstitial is doubly positive throughout the bandgap. It should be noted that the interstitial is known to be mobile at temperatures above 65 K. On the oxygen sublattice on the other hand, the vacancy is a deep double donor and thus in its neutral charge state in *n*-type material (above 2.1 eV above the valence band maximum) while the interstitial can be either neutral ($O_{i,split}$) or doubly negative ($O_{i,oct}$). When treating defect generation as a ballistic process and neglecting transitions between the two, the formation of $O_{i,oct}$ and $O_{i,split}$ will be random and thus the concentration of the two configurations will be equal. Hence, for the indicated E_F the average net effect of a Frenkel pair on the oxygen sublattice is to trap one electron.

Randomly generating Frenkel pairs on both sublattices will thus compensate *n*-type material until the Fermi level crosses the (+2/0) transition of the oxygen vacancy (2.1 eV above the valence band maximum) at which point no further change in the carrier concentration will take place. This is qualitatively consistent with the observed increase in resistivity seen for ZnO in figure 3 for displacement damage doses between 6×10^{14} MeV g^{-1} and $\sim 6 \times 10^{16}$ MeV g^{-1} .

As the dose is increased above 1.8×10^{17} MeV g^{-1} , figure 3 shows that the resistivity of ZnO starts decreasing. Employing

only the isolated intrinsic defects, as discussed above, there should be no driving force towards a lower resistivity as the Fermi level will be pinned at the deep transition level of the oxygen vacancy. However, as the dose is increased the distance between individual defects is reduced, and even though diffusion is suppressed at low temperature, the initial assumption of not forming defect complexes does no longer apply. As an example, assuming uniformly distributed point defects at a concentration of 10^{19} cm^{-3} , the average distance between each defect is on the order of 5 nm. Hence, if such concentrations of Frenkel pairs are introduced, the probability of one defect being generated in the immediate vicinity of another is high, and thus complexes can form virtually without the need for diffusion. The process behind the decreasing resistance at displacement damage doses greater than $3 \times 10^{17} \text{ MeV g}^{-1}$ for ZnO is thus believed to be the same as that responsible for the increasing resistance at lower doses, generation of Frenkel pairs. The only difference being the concentration of defects already present in the sample when a new Frenkel pair is formed. Threshold values for when the isolated point defects and complexes start to dominate the electrical characteristics of the ZnO sample are roughly 5×10^{14} and 10^{16} – $10^{17} \text{ MeV g}^{-1}$, respectively, as seen in figure 3.

In principle, the following complexes between intrinsic point defects could be considered: $V_{\text{Zn}}V_{\text{O}}$, O_{Zn} , Zn_{O} and $Zn_{\text{i}}O_{\text{i}}$, in addition to larger clusters. $Zn_{\text{i}}O_{\text{i}}$ would be a ZnO positioned interstitially which, although observed in pelletized ZnO powders [53], is not expected to be stable in thin films and is disregarded. To the best of our knowledge, no hybrid DFT data exists for the Zn antisite, Zn_{O} , hence this complex is also disregarded in the following. Furthermore, complexes involving one or more impurity atoms are also possible.

The $V_{\text{Zn}}V_{\text{O}}$ divacancy has been both theoretically and experimentally found to be stable, at least at temperatures below $200 \text{ }^\circ\text{C}$ [30, 54]. This divacancy was found to be electrically neutral in a neutron irradiated ZnO crystal, but could be excited to the +1 charge state by laser illumination at low temperatures [54]. From hybrid DFT calculations it is suggested that both the -2 and $+2$ states can also be stabilized [30]. By correlating positron annihilation spectroscopy (PAS) and *IV* measurements on oxygen irradiated ZnO thin films, Zubiaga *et al* have shown that the introduction of zinc vacancies increases the resistivity of the film [55]. They also found that, under their irradiation conditions using O-ions with an energy of 2 MeV, a maximum V_{Zn} concentration of about 2 – $5 \times 10^{18} \text{ cm}^{-3}$ could be obtained before the formation of vacancy complexes started. Increasing the dose further did not significantly change the resistivity, from which it was tentatively concluded that the vacancy complexes were electrically inactive. The details of the complexes were not discussed, but results from electron irradiation experiments of ZnO indicate that the V_{Zn} takes part in more than one type of complex [56, 57]. The onset of cluster formation as a function of dose, depends on the energy and mass of the irradiated ion, and although the exact position of the resistance peak as function of irradiation dose cannot be directly observed (due to the high resistance in the range 6×10^{15} – $1.8 \times 10^{17} \text{ MeV g}^{-1}$), our results qualitatively agree with those of Zubiaga *et al* [55]. In

the grey shaded region towards the right of figure 4 we show the effect of two complexes involving V_{Zn} on the net charge state of the material. The column labelled $V_{\text{Zn}} + V_{\text{O}}$ shows the sum of the charge states of the two defects, while the column $V_{\text{Zn}}V_{\text{O}}$ shows the charge states of the divacancy complex as computed by DFT in [30]. It is found that for Fermi levels between 2.09 and 3.2 eV above the VBM the divacancy has a higher charge state than the sum of the constituents. Hence, forming the complex can increase the carrier concentration and pull E_{F} up to $\text{VBM} + 3.2 \text{ eV}$, thus explaining the decreasing resistivity at higher doses. This complex alone will, however, not increase the carrier concentration beyond that of the as-deposited material, and other complexes are needed. The oxygen antisite O_{Zn} shown to the far right of figure 4 will not contribute since, even though it has a higher charge state than the constituent point defects throughout the band gap, it is still an acceptor, hence some other, unknown, complex must come into play.

The remaining, unexplained, feature of the ZnO curve of figure 3 is the initial decrease in resistivity at low doses. Although several studies of the dose dependent resistivity of ZnO have been made in the past [20, 49, 53, 55] this has, to the best of our knowledge, not previously been observed in this material. A possible reason is that our irradiation and *IV* measurements are performed at low temperature, while the cited works have all been performed at room temperature or above. The detailed mechanism behind this resistance drop, observed also for In_2O_3 and SnO_2 , is not clear and warrants further, dedicated, studies.

3.2. In_2O_3

The atomic structure of In_2O_3 consists of two inequivalent In sites and two different interstitial positions, thus this consequently increases the complexity of the defect structure. As a result, computing defect charge state transition levels have proven challenging and the results are heavily dependent on the details of the computation. Even qualitatively determining whether the oxygen vacancy is a deep or shallow donor is not straightforward [58], but several recent hybrid functional DFT computations have agreed that it is in fact shallow [38, 59, 60]. Due to the excellent agreement between the computed value and the experimental band gap, we will in the following refer to the defect levels found in [38], illustrated in figure 5, as the basis for discussing the In_2O_3 curve of figure 3.

For the Fermi level indicated in figure 5, a Frenkel pair on the oxygen sublattice can have a net charge state of -1 , 0 or $+1$ depending on the position of the oxygen interstitial. Assuming that the positions have equal probabilities of occupation, the averaged charge of the oxygen Frenkel pairs is thus zero. For a Frenkel pair on the indium sublattice the net charge state is negative as long as the Fermi level is higher than 0.21 eV below the CBM. Random introduction of Frenkel pairs can thus qualitatively explain the increase in resistance seen at displacement damage doses in the range 4.9×10^{14} – $2.5 \times 10^{16} \text{ MeV g}^{-1}$. As for ZnO, we argue that the decreasing resistivity at higher doses is caused by formation of defect complexes. For instance figure 5 shows that, for Fermi levels in the vicinity of the CBM, the defect reaction $V_{\text{In}}^{\text{b}} + O_{\text{i}}^{\text{c}} \rightarrow O_{\text{In}}^{\text{b}}$ will transform

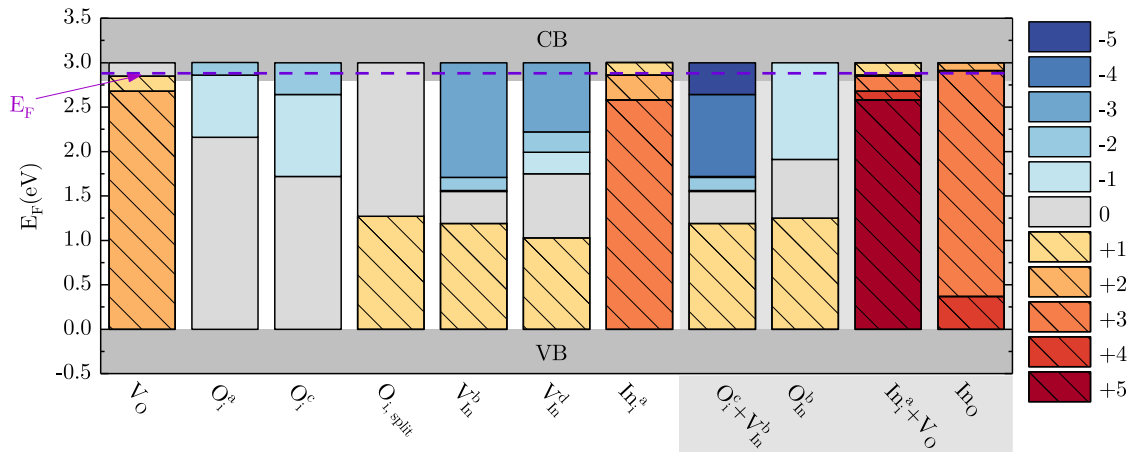


Figure 5. Thermodynamic charge states and transition levels for intrinsic defects in In_2O_3 . The estimated Fermi level before irradiation is represented by the dashed purple line 2.88 eV above the VBM. For the antisites towards the right of the figure, we show also the arithmetic sums of the charges of the constituent point defects to highlight the effect of complex formation. All the transition levels were extracted from [38] with permission.

two defects with a total charge of -3 , -4 or -5 to a complex of charge -1 , thus releasing 2, 3 or 4 electrons to the conduction band. This complex is still an acceptor, however, and does not explain why the carrier concentration after the final irradiation dose is higher than in the as-deposited sample. The indium antisite (In_O) formed by combining one $\text{In}_\text{I}^{\text{a}}$ and one oxygen vacancy, on the other hand, is a donor which, for Fermi levels within the conduction band, has a higher charge state than the constituents. This intrinsic complex could thus contribute to pushing the Fermi level deeper into the conduction band.

3.3. Ga_2O_3 and SnO_2

As seen in figure 3, the dose dependence of the resistances of Ga_2O_3 and SnO_2 behaves qualitatively different from those of In_2O_3 and ZnO . Nevertheless, if we postulate that the complexes forming at higher doses do not release the electrons trapped by the constituent point defects but rather retain their acceptor character throughout the dose range, the same general model as used above can be applied to these materials as well.

In [48], a thorough search for defects responsible for the irradiation induced resistivity in Ga_2O_3 was undertaken by deep level transient- and optical spectroscopy and DFT calculations. Their results suggest that a combination of V_{Ga} , Ga_i and Ga_O pins the Fermi level at least 0.5 eV below the CBM, thus causing its high resistivity. Positron annihilation spectroscopy has shown that isolated gallium vacancies can be formed in concentrations greater than $5 \times 10^{18} \text{ cm}^{-3}$ during film growth [61], and V_{Ga} generated from ion irradiation has also been evidenced [62]. In the latter reference it is found, however, that the V_{Ga} concentration alone is too low to account for the observed charge carrier removal rate, and it is argued that the main cause of increased resistivity is that the irradiation induced defects form neutral complexes with shallow donors. The details of these complexes are still unknown, but neutron irradiation experiments followed by deep level spectroscopy shows both a considerably increased concentration of a defect level situated 2.00 eV below the conduction band

minimum, and the introduction of a new state at 1.29 eV below the CBM [63]. These defects are correlated with a reduction in the electron concentration from $\sim 1.2 \times 10^{17} \text{ cm}^{-3}$ to $\sim 4.0 \times 10^{16} \text{ cm}^{-3}$ after irradiation to an 1 MeV equivalent dose of $1.7 \times 10^{15} \text{ cm}^{-2}$.

Figure 6 shows the defect levels calculated in [48], with the Fermi level of the as-deposited sample superimposed. If a Frenkel pair is generated on the Ga sublattice for the given Fermi level, the net charge state will be -1 , while for the oxygen sublattice it will be either 0 or -2 depending on the details of the oxygen interstitial. Assuming again equal probability of the interstitial sites, the average charge state will be -1 and thus random generation of Frenkel pairs on both sublattices is expected to reduce the carrier concentration and increase the resistivity of the sample. Comparing the charge states of individual gallium interstitials, oxygen vacancies and gallium antisites, it is found that the formation of a gallium antisite from its constituent point defects decreases its charge state for all the oxygen sites. Hence, this particular complex will not reduce the resistance if formed at high doses, and unless other, donor like, complexes form the carrier concentration will remain low and the resistivity high as observed in figure 3.

For SnO_2 it has been suggested that removal of substitutional hydrogen as well as introduction of intrinsic acceptors, e.g. V_{Sn} , O_i or O_{Sn} , is responsible for the dose dependent increase in resistivity [64]. Like for ZnO , DFT calculations predict a deep ($+2/0$) transition level for V_O , while tin interstitials and antisites are expected to be positively ionized throughout the band gap [65]. Based on this, Frenkel pairs on the tin sublattice are expected to give zero net contribution to the carrier concentration. On the oxygen sublattice, the deep V_O means that Fermi levels close to the CBM will cause a surplus of electrically active acceptors to form, hence explaining the increasing resistivity at doses greater than $1.5 \times 10^{15} \text{ MeV g}^{-1}$. In addition, the dual valency of Sn can possibly also play a role. If the irradiation somehow induces a reduction of Sn^{4+} to Sn^{2+} this will trap two electrons and contribute to the observed increase in resistivity.

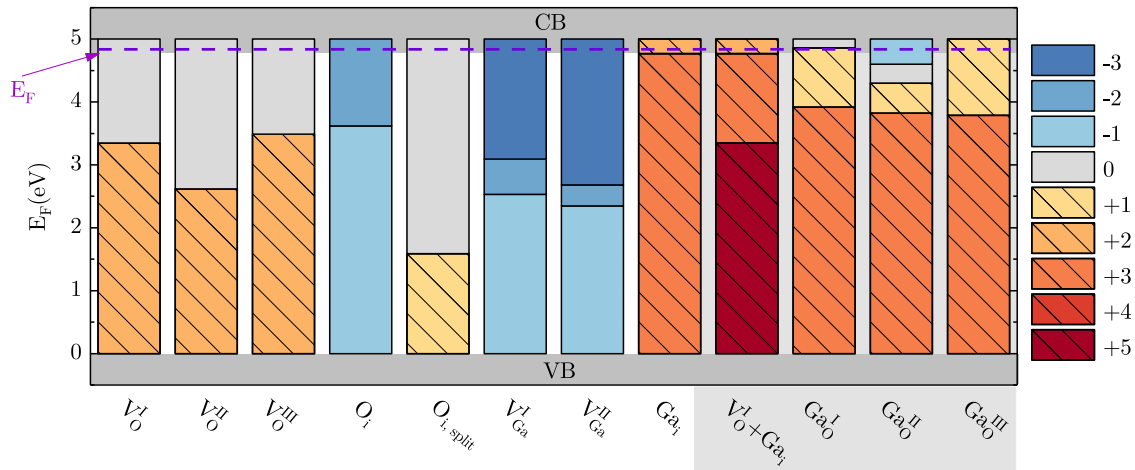


Figure 6. Thermodynamic charge states and their transition levels for intrinsic defects in Ga_2O_3 . The estimated Fermi level before irradiation is represented by the dashed purple line 4.85 eV above the VBM. For the Ga_O^1 antisite towards the right of the figure, we show also the arithmetic sum of the constituent V_O^1 and Ga_i point defects. All the transition levels were sourced from [48] (licensed under a Creative Commons Attribution (CC BY) license).

As Ga_2O_3 and SnO_2 have a markedly different dose dependent resistance behaviour from the other three materials studied in this paper it is interesting to note another feature where they are different. Unlike most other metal oxides, Ga_2O_3 and SnO_2 have two possible positions for the hydrogen interstitial. One position disrupts the anion-cation bonds of the host material, and gives the $\text{H}(+/-)$ level associated with the CNL, as found in other materials as well [13]. The other configuration places the hydrogen on an oxygen lone-pair and may give an energetically favourable donor state well within the conduction band [66]. As discussed in [64] it is possible that removal of such pre-existing hydrogen donors contribute to the increasing resistance with irradiation.

3.4. CdO

For CdO only a minor change in the resistivity is observed across the dose range. This can possibly be explained by hybrid-DFT calculations, which indicate that all the intrinsic defects, as well as interstitial and substitutional hydrogen, will be either neutral or in a positive charge state until the Fermi level is about 0.6 eV above the CBM [67]. A likely reason why the introduction of such positively charged defects does not considerably decrease the resistivity could be a simultaneous, comparable decrease in mobility. The Hall effect results indeed show that irradiation to a displacement damage dose of $1.7 \times 10^{18} \text{ MeV g}^{-1}$ yields an increase in electron concentration from 1.34×10^{19} to $1.65 \times 10^{20} \text{ cm}^{-3}$ and a decrease in mobility from 285 to $22.9 \text{ cm}^2 (\text{V s})^{-1}$ at a temperature of 70 K, as illustrated in figure 2. It should be noted that the sample was stored at room temperature for approximately two weeks between the *IV*- and Hall effect measurements. Diffusion and/or defect reactions may in principle have taken place during this time, hence the carrier concentration and mobility measured by the Hall effect may differ somewhat from their values during the *IV* measurements. Nevertheless, these values seem to explain the observation that the resistance

is close to constant as a function of irradiation dose for CdO in figure 3.

To summarize, for displacement damage doses greater than approximately $5 \times 10^{14} \text{ MeV g}^{-1}$ three types of behaviour are possible. (i) If the net charge state of the point defects and their complexes is positive the carrier concentration will increase. This tends to reduce the resistivity, with a magnitude dependent on the evolution of the mobility. If the mobility decreases comparably to the increase in carrier concentration, the resistivity will remain constant, as seen for CdO. (ii) If the net charge state of the point defects is negative, while that of their complexes is positive, the resistivity will initially increase followed by a decrease as the dose is increased further, resulting in a peak behaviour. This is seen for In_2O_3 and ZnO. (iii) If the net charge state of the point defects and their complexes is negative, the resistivity will increase and remain high for arbitrarily high doses, as observed for Ga_2O_3 and SnO_2 .

This model assumes that the irradiation forms Frenkel pairs on all sublattices of the sample and that, at low doses, the point defects do not agglomerate into complexes. Further, we assume that complexes are able to form as the dose, and consequently the point defect concentration, increases above a threshold value. Depending on the charge states of the defects and their complexes, this can result in a 2-stage behaviour of the defect concentration dependent Fermi level. In cases (i) and (iii) above, the Fermi level will change monotonically with defect concentration towards the CNL, and in these cases our model is identical to the ADM. In case (ii), as we observe for materials ZnO, In_2O_3 and CdO, a more involved defect/complex balance is observed. This behavior is found when the overall charge balance is changed when going from isolated defects towards the formation of defect complexes. We believe the model to be general and applicable to any semiconducting material. At present it cannot explain the decreasing resistivity seen for In_2O_3 , SnO_2 and ZnO at the lowest doses, and investigating this requires further studies outside the scope of this work.

4. Conclusions

In conclusion, it has been found that some materials can be made heavily *n*-type by introducing intrinsic defects, whereas others become highly resistive. The evolution of sample resistance with dose has been found to proceed along one of three possible routes. Ga₂O₃ and SnO₂ irradiated to displacement damage doses of 5.6×10^{18} or 1.6×10^{18} MeV g⁻¹, respectively, were found to be highly resistive. For In₂O₃ and ZnO the irradiation ultimately turned the samples less resistive than in their respective as-deposited states, but a more resistive state is observed at intermediate doses. The resistance of CdO changes only weakly with irradiation, probably caused by complementary changes in carrier concentration and mobility. For CdO, In₂O₃ and ZnO, the irradiation was found to increase the carrier concentration, and for In₂O₃ the mobility was increased as well. This work shows that the combined charge state of randomly introduced Frenkel pairs can explain the evolution of the charge carrier concentration as function of ion irradiation dose. For all the samples except SnO₂ the change in carrier concentration after irradiation is qualitatively in accordance with the respective charge neutrality levels [66].

Furthermore, the formation of defect complexes is found to be important in order to understand the behaviour at displacement damage doses exceeding about 10^{16} MeV g⁻¹, even in low temperature experiments due to the high density of generated defects. Thus, this work contributes as a further development of the amphoteric defect model for defect evolution in irradiated samples. Finally, it should be noted that the differing behaviour between the various materials is expected to be caused by differences in their thermodynamic defect charge state transitions. In particular, the position of the oxygen vacancy relative to the divacancy or other small complexes is believed to play a major role, thus showing both the importance of defect complexes in general and also the potential for using hybrid DFT calculations to explain the defect evolution in a range of wide band-gap oxides.

Acknowledgments

The authors acknowledge Holger Hochmuth of the University of Leipzig for growing the Ga₂O₃ and In₂O₃ films, Rodrigo Martinez Gazoni and Roger J Reeves of the University of Canterbury for the growth of the SnO₂ films, and Viktor Bobal of the University of Oslo for operating the ion implanter. The Research Council of Norway is acknowledged for the support to the Norwegian Micro- and Nano-Fabrication Facility, NorFab, project number 245963, and the FOXHOUND project. The Norwegian Nano Network and UiO:Energy are gratefully acknowledged for travel and conference support.

ORCID iDs

J Borgersen  <https://orcid.org/0000-0002-4350-2233>

L Vines  <https://orcid.org/0000-0001-5759-7192>

Y K Frodason  <https://orcid.org/0000-0001-9151-2084>

A Kuznetsov  <https://orcid.org/0000-0003-1822-9850>

H von Wenckstern  <https://orcid.org/0000-0002-3936-275X>

M Grundmann  <https://orcid.org/0000-0001-7554-182X>

M Allen  <https://orcid.org/0000-0001-8786-6429>

J Zúñiga-Pérez  <https://orcid.org/0000-0002-7154-641X>

K M Johansen  <https://orcid.org/0000-0002-6268-1740>

References

- [1] Özgür Ü, Alivov Y I, Liu C, Teke A, Reshchikov M A, Doğan S, Avrutin V, Cho S-J and Morkoç H 2005 A comprehensive review of ZnO materials and devices *J. Appl. Phys.* **98** 041301
- [2] Bierwagen O 2015 Indium oxide—a transparent, wide-band gap semiconductor for (opto)electronic applications *Semicond. Sci. Technol.* **30** 024001
- [3] Chandiramouli R and Jeyaprakash B G 2013 Review of CdO thin films *Solid State Sci.* **16** 102–10
- [4] Das S and Jayaraman V 2014 SnO₂: a comprehensive review on structures and gas sensors *Prog. Mater. Sci.* **66** 112–255
- [5] von Wenckstern H 2017 Group-III sesquioxides: growth, physical properties and devices *Adv. Electron. Mater.* **3** 1600350
- [6] Alkauskas A, McCluskey M D and Van de Walle C G 2016 Tutorial: defects in semiconductors—Combining experiment and theory *J. Appl. Phys.* **119** 181101
- [7] Walukiewicz W 1988 Fermi level dependent native defect formation: consequences for metal–semiconductor and semiconductor–semiconductor interfaces *J. Vac. Sci. Technol. B: Microelectron. Process. Phenom.* **6** 1257–62
- [8] Walukiewicz W 1987 Mechanism of Schottky barrier formation: the role of amphoteric native defects *J. Vac. Sci. Technol. B: Microelectron. Process. Phenom.* **5** 1062–7
- [9] King P D C, Veal T D, Jefferson P H, Zúñiga-Pérez J, Muñoz-Sanjosé V and McConville C F 2009 Unification of the electrical behavior of defects, impurities, and surface states in semiconductors: virtual gap states in CdO *Phys. Rev. B* **79** 035203
- [10] King P D C, Veal T D, Payne D J, Bourlange A, Egdell R G and McConville C F 2008 Surface electron accumulation and the charge neutrality level in In₂O₃ *Phys. Rev. Lett.* **101** 116808
- [11] Mönch W 1996 Empirical tight-binding calculation of the branch-point energy of the continuum of interface-induced gap states *J. Appl. Phys.* **80** 5076–82
- [12] Schleife A, Fuchs F, Rödl C, Furthmüller J and Bechstedt F 2009 Branch-point energies and band discontinuities of III-nitrides and III/II-oxides from quasiparticle band-structure calculations *Appl. Phys. Lett.* **94** 012104
- [13] Van de Walle C G and Neugebauer J 2003 Universal alignment of hydrogen levels in semiconductors, insulators and solutions *Nature* **423** 626–8
- [14] Tersoff J 1984 Theory of semiconductor heterojunctions: the role of quantum dipoles *Phys. Rev. B* **30** 4874–7
- [15] Brudnyi V N, Grinyaev S N and Kolin N G 2003 Electronic properties of irradiated semiconductors. a model of the Fermi level pinning *Semiconductors* **37** 537–45
- [16] Falabretti B and Robertson J 2007 Electronic structures and doping of SnO₂, CuAlO₂, and CuInO₂ *J. Appl. Phys.* **102** 123703
- [17] Amini M N, Saniz R, Lamoén D and Partoens B 2011 Hydrogen impurities and native defects in CdO *J. Appl. Phys.* **110** 063521
- [18] Speaks D T, Mayer M A, Yu K M, Mao S S, Haller E E and Walukiewicz W 2010 Fermi level stabilization energy in cadmium oxide *J. Appl. Phys.* **107** 113706
- [19] Vines L, Bhodoo C, von Wenckstern H and Grundmann M 2018 Electrical conductivity of In₂O₃ and Ga₂O₃ after low temperature ion irradiation; implications for intrinsic defect

- formation and charge neutrality level *J. Phys.: Condens. Matter.* **30** 025502
- [20] Kucheyev S O, Deenapanray P N K, Jagadish C, Williams J S, Yano M, Koike K, Sasa S, Inoue M and Ogata K-i 2002 Electrical isolation of ZnO by ion bombardment *Appl. Phys. Lett.* **81** 3350–2
- [21] Kucheyev S O, Williams J S, Jagadish C, Zou J, Evans C, Nelson A J and Hamza A V 2003 Ion-beam-produced structural defects in ZnO *Phys. Rev. B* **67** 094115
- [22] Ziegler J F, Biersack J P and Littmark U 1985 *The Stopping and Range of Ions in Solids* (New York: Pergamon)
- [23] Krukau A V, Vydrov O A, Izmaylov A F and Scuseria G E 2006 Influence of the exchange screening parameter on the performance of screened hybrid functionals *J. Chem. Phys.* **125** 224106
- [24] Blöchl P E 1994 Projector augmented-wave method *Phys. Rev. B* **50** 17953–79
- [25] Kresse G and Furthmüller J 1996 Efficient iterative schemes for *ab initio* total-energy calculations using a plane-wave basis set *Phys. Rev. B* **54** 11169–86
- [26] Oba F, Togo A, Tanaka I, Paier J and Kresse G 2008 Defect energetics in ZnO: a hybrid Hartree–Fock density functional study *Phys. Rev. B* **77** 245202
- [27] Freysoldt C, Grabowski B, Hickel T, Neugebauer J, Kresse G, Janotti A and Van de Walle C G 2014 First-principles calculations for point defects in solids *Rev. Mod. Phys.* **86** 253–305
- [28] Kumagai Y and Oba F 2014 Electrostatics-based finite-size corrections for first-principles point defect calculations *Phys. Rev. B* **89** 195205
- [29] Lyons J L, Varley J B, Steiauf D, Janotti A and Van de Walle C G 2017 First-principles characterization of native-defect-related optical transitions in ZnO *J. Appl. Phys.* **122** 035704
- [30] Frodason Y K, Johansen K M, Alkauskas A and Vines L 2019 Negative-*u* and polaronic behavior of the Zn–O divacancy in ZnO *Phys. Rev. B* **99** 174106
- [31] Look D C 1989 *Electrical Characterization of GaAs Materials and Devices* (New York: Wiley)
- [32] Farahani S K V, Muñoz-Sanjosé V, Zúñiga-Pérez J, McConville C F and Veal T D 2013 Temperature dependence of the direct bandgap and transport properties of CdO *Appl. Phys. Lett.* **102** 022102
- [33] Look D C, Mosbacker H L, Strzhemechny Y M and Brillson L J 2005 Effects of surface conduction on Hall-effect measurements in ZnO *Superlattices Microstruct.* **38** 406–12 E-MRS 2005 Symp. G: ZnO and Related Materials
- [34] Roro K T, Kassier G H, Dangbegnon J K, Sivaraya S, Westraadt J E, Neethling J H, Leitch A W R and Botha J R 2008 Temperature-dependent Hall effect studies of ZnO thin films grown by metalorganic chemical vapour deposition *Semicond. Sci. Technol.* **23** 055021
- [35] Karsthof R, von Wenckstern H, Zúñiga-Pérez J, Deparis C and Grundmann M 2020 Nickel oxide-based heterostructures with large band offsets *Phys. Status Solidi b* **257** 1900639
- [36] Farahani S K V, Veal T D, King P D C, Zúñiga-Pérez J, Muñoz-Sanjosé V and McConville C F 2011 Electron mobility in CdO films *J. Appl. Phys.* **109** 073712
- [37] Kim R, Wang X and Lundstrom M 2008 *Notes on Fermi-Dirac Integrals* (<https://arxiv.org/ftp/arxiv/papers/0811/0811.0116.pdf>)
- [38] Chatratin I, Sabino F P, Reunchan P, Limpijumngong S, Varley J B, Van de Walle C G and Janotti A 2019 Role of point defects in the electrical and optical properties of In₂O₃ *Phys. Rev. Mater.* **3** 074604
- [39] Farahani S K V, Veal T D, Mudd J J, Scanlon D O, Watson G W, Bierwagen O, White M E, Speck J S and McConville C F 2014 Valence-band density of states and surface electron accumulation in epitaxial SnO₂ films *Phys. Rev. B* **90** 155413
- [40] Peelaers H and Van de Walle C G 2015 Brillouin zone and band structure of β -Ga₂O₃ *Phys. Status Solidi b* **252** 828–32
- [41] Feneberg M, Nixdorf J, Lidig C, Goldhahn R, Galazka Z, Bierwagen O and Speck J S 2016 Many-electron effects on the dielectric function of cubic In₂O₃: effective electron mass, band nonparabolicity, band gap renormalization, and Burstein–Moss shift *Phys. Rev. B* **93** 045203
- [42] Fuchs F and Bechstedt F 2008 Indium-oxide polymorphs from first principles: quasiparticle electronic states *Phys. Rev. B* **77** 155107
- [43] Look D C, Farlow G C, Reunchan P, Limpijumngong S, Zhang S B and Nordlund K 2005 Evidence for native-defect donors in *n*-type ZnO *Phys. Rev. Lett.* **95** 225502
- [44] Hupfer A, Bhoodoo C, Vines L and Svensson B G 2016 Formation and annihilation of E4 centers in ZnO: influence of hydrogen *J. Appl. Phys.* **119** 181506
- [45] Messenger S R, Burke E A, Summers G P, Xapsos M A, Walters R J, Jackson E M and Weaver B D 1999 Nonionizing energy loss (NIEL) for heavy ions *IEEE Trans. Nucl. Sci.* **46** 1595–602
- [46] Loferski J J and Rappaport P 1958 Radiation damage in Ge and Si detected by carrier lifetime changes: damage thresholds *Phys. Rev.* **111** 432–9
- [47] Svensson B G, Jagadish C, Hallén A and Lalita J 1997 Generation of vacancy-type point defects in single collision cascades during swift-ion bombardment of silicon *Phys. Rev. B* **55** 10498–507
- [48] Ingebrigtsen M E, Kuznetsov A Y, Svensson B G, Alfieri G, Mihaila A, Badstübner U, Perron A, Vines L and Varley J B 2019 Impact of proton irradiation on conductivity and deep level defects in β -Ga₂O₃ *APL Mater.* **7** 022510
- [49] Kucheyev S O, Jagadish C, Williams J S, Deenapanray P N K, Yano M, Koike K, Sasa S, Inoue M and Ogata K-i 2003 Implant isolation of ZnO *J. Appl. Phys.* **93** 2972–6
- [50] Kato Y, Shimada T, Shiraki Y and Komatsubara K F 1974 Electrical conductivity of disordered layers in GaAs crystal produced by ion implantation *J. Appl. Phys.* **45** 1044–9
- [51] Wendler E and Wesch W 2016 Primary processes of damage formation in semiconductors *Ion Beam Modification of Solids: Ion-Solid Interaction and Radiation Damage* ed W Wesch and E Wendler (Berlin: Springer International Publishing) pp 189–241 ch 5
- [52] Frodason Y K, Johansen K M, Bjørheim T S, Svensson B G and Alkauskas A 2017 Zn vacancy as a polaronic hole trap in ZnO *Phys. Rev. B* **95** 094105
- [53] Pal S *et al* 2018 Clustered vacancies in ZnO: chemical aspects and consequences on physical properties *J. Phys. D: Appl. Phys.* **51** 105107
- [54] Holston M S, Golden E M, Kananen B E, McClory J W, Giles N C and Halliburton L E 2016 Identification of the zinc–oxygen divacancy in ZnO crystals *J. Appl. Phys.* **119** 145701
- [55] Zubiaga A, Tuomisto F, Coleman V A, Tan H H, Jagadish C, Koike K, Sasa S, Inoue M and Yano M 2008 Mechanisms of electrical isolation in O⁺-irradiated ZnO *Phys. Rev. B* **78** 035125
- [56] Tuomisto F, Saarinen K, Look D C and Farlow G C 2005 Introduction and recovery of point defects in electron-irradiated ZnO *Phys. Rev. B* **72** 085206
- [57] Johansen K M, Tuomisto F, Makkonen I and Vines L 2017 Formation of Zn- and O-vacancy clusters in ZnO through deuterium annealing *Mater. Sci. Semicond. Process.* **69** 23–7 ZnO-based materials and applications
- [58] Reunchan P, Zhou X, Limpijumngong S, Janotti A and Van de Walle C G 2011 Vacancy defects in indium oxide: an *ab initio* study *Curr. Appl. Phys.* **11** S296–300
- [59] Ágoston P, Albe K, Nieminen R M and Puska M J 2009 Intrinsic *n*-type behavior in transparent conducting oxides: a comparative hybrid-functional study of In₂O₃, SnO₂, and ZnO *Phys. Rev. Lett.* **103** 245501

- [60] Buckeridge J *et al* 2018 Deep vs shallow nature of oxygen vacancies and consequent *n*-type carrier concentrations in transparent conducting oxides *Phys. Rev. Mater.* **2** 054604
- [61] Korhonen E, Tuomisto F, Gogova D, Wagner G, Baldini M, Galazka Z, Schewski R and Albrecht M 2015 Electrical compensation by Ga vacancies in Ga₂O₃ thin films *Appl. Phys. Lett.* **106** 242103
- [62] Polyakov A Y *et al* 2018 Defects responsible for charge carrier removal and correlation with deep level introduction in irradiated β -Ga₂O₃ *Appl. Phys. Lett.* **113** 092102
- [63] Farzana E, Chaiken M F, Blue T E, Arehart A R and Ringel S A 2019 Impact of deep level defects induced by high energy neutron radiation in β -Ga₂O₃ *APL Mater.* **7** 022502
- [64] Gupta S, Singh F, Lalla N P and Das B 2017 Swift heavy ion irradiation induced modifications in structural, microstructural, electrical and magnetic properties of Mn doped SnO₂ thin films *Nucl. Instrum. Methods Phys. Res. Sect. B: Beam Interact. Mater. Atoms* **400** 37–57
- [65] Janotti A and Van de Walle C G 2011 LDA + U and hybrid functional calculations for defects in ZnO, SnO₂, and TiO₂ *Phys. Status Solidi b* **248** 799–804
- [66] Swallow J E N, Varley J B, Jones L A H, Gibbon J T, Piper L F J, Dhanak V R and Veal T D 2019 Transition from electron accumulation to depletion at β -Ga₂O₃ surfaces: the role of hydrogen and the charge neutrality level *APL Mater.* **7** 022528
- [67] Burbano M, Scanlon D O and Watson G W 2011 Sources of conductivity and doping limits in CdO from hybrid density functional theory *J. Am. Chem. Soc.* **133** 15065–72